Inherent Smoothness of Intensity Patterns for Intensity Modulated Radiation Therapy Generated by Simultaneous Projection Algorithms

Y. Xiao[1], D. Michalski[1], Y. Censor[2] and J. M. Galvin[1]

[1] *Medical Physics Division,*

Radiation Oncology Department,

Thomas Jefferson University Hospital,

10th and Locust Streets, Philadelphia,

PA. 19107, USA.

({ying.xiao, darek.michalski, james.galvin}@mail.tju.edu).

[2] *Department of Mathematics,*

University of Haifa, Mt. Carmel,

Haifa 31905, Israel.

(yair@math.haifa.ac.il).

(May, 2004)

Abstract

The efficient delivery of intensity modulated radiation therapy (IMRT) dependends on finding optimized beam intensity patterns that produce dose distributions, which meet given constraints for the tumor as well as any critical organs to be spared. Many optimization algorithms that are used for beamlet-based inverse planning are susceptible to large variations of neighboring intensities. Accurately delivering an intensity pattern with a large number of extrema can prove impossible given the mechanical limitations of standard MLC delivery systems. In this study, we apply Cimmino's simultaneous projection algorithm to the beamlet-based inverse planning problem, modeled mathematically as a system of linear inequalities. We show that using this method allows us to arrive at a smoother intensity pattern. Including non-linear terms in the simultaneous projection algorithm to deal with dose-volume histogram (DVH) constraints does not compromise this property from our experimental observation. The smoothness properties are compared with those from other optimization algorithms which include simulated annealing and gradient descent method. The simultaneous property of these algorithms is ideally suited to parallel computing technologies.

I. INTRODUCTION

Intensity modulated radiation therapy (IMRT) with two-dimensional (2D) modulated beams obtained from inverse planning methods makes it possible to create dose distributions that conform to both convex and concave shaped targets(Haas 1999). The success of such a radiation treatment technique depends as much on the accurate and efficient delivery of the intensity profiles as on the derivation of such intensities from the inverse planning process. The inverse planning process starts with the specification of constraints on required and permitted dose distributions to target and critical organs, and usually the assignment of *importance weights* to these constraints. The constraints may be modeled as a system of linear and/or non-linear inequalities, e.g., Starkschall (Starkschall 1984), Webb, Convery and Evans (Webb, Convery and Evans 1998), Xia and Verhey (Xia and Verhey 1998), Xiao *et al.* (Xiao, Galvin, Hossain and Valicenti 2000) and Bednarz et al(Bednarz, Michalski, Houser, Huq, Xiao, Anne and Galvin 2002), with or without an objective (cost) function imposed on them.

A basic difficulty, associated with this approach for many of the planning algorithms, is that the beam intensities can exhibit complex patterns due to the fact that the whole optimization process is susceptible to high-frequency spatial fluctuations. The accurate and efficient delivery of these irregular beam intensities remains a practical clinical challenge. *Smooth intensities*, i.e., intensities which exhibit moderate changes between adjacent beamlets, are preferable for the following reasons: (i) they are not sensitive to treatment uncertainties; (ii) they may be easier to generate under the limitations of the delivery system; they require fewer segments for multiple-static-fields (MSF) delivery with multileaf collimator (MLC) (Xia and Verhey 1998); they may be more favorable to dynamic delivery with MLCs (DMLC) with reduced “beam-on” time ((Webb et al. 1998) and (Spirou, Fournier-Bidoz, Yang, Chui and Ling 2001)).

Extensive research has been concentrated on the generation of smooth beamlet intensity patterns. Stochastic inverse planning processes are being adjusted to redistribute the beamlet intensity patterns into smoother beams. Through the iteration process filters are applied to constrain the intensity distributions (Webb et al. 1998). Two methods are commonly employed for treatment planning systems which use gradient inverse planning algorithm (Spirou et al. 2001): (i) smoothing applied outside the objective function; (ii) inclusion of a term representing smoothness of the profiles in the objective function used in the optimization process. Smoothing was also implemented within the objective function by imposing a minimal surface smoothing constraint, e.g. by Alber and Nusslin (Alber and Nusslin 2000). All these approaches yield acceptable dose distributions with smoother intensity patterns.

Historically, the inverse problem of a fully discretized model in IMRT has been formulated and solved as a mathematical *feasibility problem* by Altschuler and Censor (Altschuler and Censor 1984) and Cimmino’s algorithm was proposed for this problem by Censor, Altschuler and Powlis in (Censor, Altschuler and Powlis 1988b) and (Powlis, Altschuler, Censor and Buhle 1989). Cimmino’s algorithm has been shown to be effective and efficient for solving a system of inequalities resulting from the full discretization of the problem. In the present study we demonstrate experimentally that, for feasible problems, the feasible solutions obtained from simultaneous Cimmino-type algorithms lead to very smooth intensity patterns without need for any external filtering. Our experiments show that this smoothness property is inherent to this class of algorithms. We describe the implementation of such a Cimmino algorithm to the three-dimensional (3D) beamlet-based inverse planning system and compare the dose and intensity distributions with a commercially available beamlet-based inverse planning system. The smoothness of the solutions obtained by Cimmino's algorithm is clearly demonstrated. In order to accommodate DVH dose objectives in the simultaneous projection algorithm, non-linear terms have to be introduced in the modeling and iteration process. However, from our experimental observation, the smoothness quality of the resulting intensity patterns are comparable to those from the Cimmino's algorithm. Dose distribution and intensity patterns from this algorithm are also included in the comparison.

This inherent smoothness of solutions obtained by Cimmino's algorithm is another advantageous property of this algorithm, that we have recently studied in (Xiao, Censor, Michalski and Galvin 2003). If initialized at zero, the algorithm always generates a sequence which converges to a very good approximation of the least-intensity feasible (LIF) solution. The property of having least-squared values of the intensities naturally translates into smoother distributions without extreme irregularities.

The paper is laid out as follows. In Section II we review the fully-discretized model and the feasibility approach, with/without DVH objectives implementation. The fully simultaneous (Cimmino) algorithm and the variation of the algorithm incorporating DVH objectives are described in Section III and , in Section IV, we discuss the relationship between a few iterative algorithms for inverse treatment planning. Following a description of our experimental setup, in Section V, we present our results (Section VI) and discuss them (Section VII). We conclude in Section VII.

II. THE SIMULTANEOUS PROJECTION ALGORITHM

The fully discretized feasibility model is included in the appendix.

In this section we discuss briefly some relevant projection algorithms and put the specific algorithm that we use here in context. We also describe how the algorithm that we use is related to the class of gradient methods that were used in the field of IMRT.

Projection algorithms employ projections onto convex sets with the underlying philosophy that whenever an intersection of a family of given convex sets is considered then performing projections onto the individual members of the family of sets is easier than performing a projection onto the intersection of sets (Hiriart-Urruty and Lemarechal 2001, Chapter A, Section 3). The *linear feasibility problem* (LFP), presented in the previous section, is a special instance of the convex feasibility problem (CFP) where the convex sets are the half-spaces described by the inequalities in (25). Let R^m be the m-dimensional Euclidean space and let $C_1, C_2, \ldots, C_n$, be nonempty closed convex subsets of R^m. The *convex feasibility problem* is to find a point $x^* \in C := \cap_{j=1}^{n} C_j$. If $C \neq \emptyset$ the problem is *consistent*, otherwise it is *inconsistent*.

The well-known "Projections Onto Convex Sets" (POCS) algorithm for the convex feasibility problem is a *sequential* projection algorithm (Stark and Yang 1998). Starting from an arbitrary initial point $x^0 \in R^m$, the POCS algorithm's iterative step for calculation of the next iterate x^{k+1} from the current one x^k is

$$x^{k+1} = x^k + \lambda_k (P_{C_{j(k)}}(x^k) - x^k), \tag{1}$$

where $\{\lambda_k\}_{k\geq 0}$ are *relaxation parameters* and $\{j(k)\}_{k\geq 0}$ is a *control sequence*, $1 \leq j(k) \leq n$, for all $k \geq 0$, which determines the index of the individual set $C_{j(k)}$ onto which the current iterate x^k is projected. A commonly used control is the *cyclic control* in which $j(k) = k \bmod n + 1$, but other controls are also available (Censor and Zenios 1997, Definition 5.1.1). The simultaneous counterpart of (1) is the, so-called, Cimmino algorithm for the convex feasibility problem. Cimmino (Cimmino 1938) originally invented it for the solution of linear equations, i.e., a system of the form $\langle a^j, x \rangle = d_j, \text{ for all } j = 1, 2, \cdots, n$, and originally used *reflections* instead of projections. Auslender (Auslender 1976) generalized Cimmino's idea to convex sets. Adding to Auslender's algorithm relaxation parameters $\{\lambda_k\}_{k\geq 0}$ and weights of importance $\{w_j\}_{j=1}^{n}$, such that $w_j > 0$ and $\sum_{j=1}^{n} w_j = 1$, one arrives at the algorithmic iterative step:

$$x^{k+1} = x^k + \lambda_k(\sum_{j=1}^{n} w_j P_{C_j}(x^k) - x^k). \tag{2}$$

For half-spaces as constraints sets, i.e.,

$$C_j = \{x \in R^m \mid \langle a^j, x\rangle \leq d_j\}, \text{ for all } j = 1, 2, \cdots, n, \tag{3}$$

the simultaneous projections methods of Cimmino for the LFP (26)(Censor et al. 1988b) and non-linear DVH terms (28)(Michalski, Xiao, Censor and Galvin 2004) are as follows :

Algorithm 1 Cimmino's Algorithm (CIM), and the algorithm dealing with DVH constraints (CIM-DVH).

Initialization: *$x^0 \in R^m$ is arbitrary.*

Importance Weights: *These are user-chosen positive real numbers $w_j > 0$, for all $j = 1, 2, \cdots, n$, with $\sum_{j=1}^{n} w_j = 1$.*

Iterative Step: *Given x^k, calculate the next iterate x^{k+1} by the formula*

$$x^{k+1} = x^k + \lambda_k \sum_{j=1}^{n} w_j c_j(x^k) a^j, \tag{4}$$

where

$$c_j(x^k) = \min(0, \frac{d_j - \langle a^j, x^k\rangle}{\|a^j\|^2}), \tag{5}$$

and go back to the beginning of the Iterative Step ($\|\cdot\|$ stands for the Euclidean norm).

Relaxation Parameters: *λ_k are user-chosen real numbers such that $\varepsilon \leq \lambda_k \leq 2 - \varepsilon$, for all $k \geq 0$, with some, arbitrarily small $\varepsilon > 0$.*

Cimmino's algorithm converges regardless of the consistency of the system of inequalities (26), i.e., in the inconsistent case, when there is no solution to the system, the CIM algorithm still generates convergent sequences $\{x^k\}_{k\geq 0}$ of beamlet intensities which converge to a minimum value of a *proximity function*

$$F(x) := (1/2) \sum_{j=1}^{n} \|x - P_{C_j}(x)\|^2, \tag{6}$$

which measures the sum of the squares of the distances to all inequalities of the system (Byrne and Censor 2001). In addition, CIM is a simultaneous algorithm whose operations can be performed on a parallel computer.

The iterative step for the additional non-linear inequalities is different from that of equation 4 (Michalski et al. 2004). The algorithm is referred to as CIM-DVH for clarity throughout the document. The gradient of g_t (equation 28), ∂g_t, is utilized:

$$x^{k+1} = x^k + \lambda_k(\sum_{t=1}^{T} w_t Y_t - x^k), \text{ where,} \tag{7}$$

$$Y_t = x^k - \frac{\partial g_t(x^k) \times \max(0, g_t(x^k))}{\|\partial g_t(x^k)\|^2} \tag{8}$$

The simultaneous property is retained in these iterations for dose-volume constraint implementation.

III. RELATED ITERATIVE ALGORITHMS FOR INVERSE TREATMENT PLANNING

The sequential POCS algorithm (1) for the linear feasibility problem (25) arising in the full discretization approach to the inverse problem of RTTP was first used in (Censor, Altschuler and Powlis 1988a) where it was called "the relaxation method of Agmon, Motzkin and Schoenberg (AMS)". Later it was used by Lee *et al.* (Lee, Cho, II and Oh 1997) and Cho *et al.* (Cho, Lee, Marks, Redstone and Oh 1997), (Cho, Lee, Marks, Oh, Sutlief and Phillips 1998). Both the sequential POCS and the simultaneous Cimmino algorithm are special cases of the more general iterative scheme called Block-Iterative Projections (BIP) which appeared in (Aharoni and Censor 1989) (Censor and Zenios 1997, Section 5.6). The BIP scheme allows processing of subsets of constraints other than a single constraint at a time (as in POCS) or all constraints at a time (as in Cimmino's algorithm). An excellent review on projection methods for convex feasibility problems is done by Bauschke and Borwein (Bauschke and Borwein 1996). A state of the art snap shot of ongoing research in this field is included in (Butnariu, Censor and Reich 2001). Cho and Marks II (Cho and Marks 2000) used the POCS method to include MLC hardware constraints in the IMRT model. The Cimmino algorithm was also used by Kolmonen, Trevo and Lahtinen (Kolmonen, Trevo and Lahtinen 1998) in conjunction with continuous approximation for the dose deposition kernel.

Recent publications report on the experimental finding that the initial practical convergence of Cimmino's algorithm can be accelerated by using relaxation parameters λ_k in (4) which are larger then the value $\lambda_k = 2$(Höffner, Decker, Schmidt, Herbig, Ritter and Wiss 1996)(Michalski et al. 2004). Wu *et al.* (Wu, Jeraj, Lu and Mackie 2004), also used the possibility to accelerate the Cimmino algorithm by overrelaxation within their work on using the algorithm for adaptive radiotherapy.

The comparisons made by the group of Cho, Marks II, *et al.* have revealed advantages of [the sequential] projections onto convex sets (POCS) method over simulated annealing. They found that more uniform target dose distributions were obtained with POCS method as compared with the simulated annealing technique using a quadratic objective function. Also it was noted that the beam intensity profiles generated by the POCS method correspond more closely to the target-organ geometry than those produced by the simulated annealing method(Cho et al. 1997, p. 312). They also found that the convex projection method can find solutions in much shorter time with minimal user interaction(Cho et al. 1998, p. 442).

Of particular interest is the precise relationship between Cimmino's algorithm and gradient and gradient-like iterative algorithms, such as the iterative algorithms that were used by Bortefeld *et al.* (Bortfeld, Bürkelbach, Boesecke and Schlegel 1990), Xing and Chen (Xing and Chen 1996), Xing *et al.* (Xing, Hamilton, Spelbring, Pelizzari, Chen and Boyer 1998), Spirou and Chui (Spirou and Chui 1998). A precise mathematical comparative analysis has not yet been done, but partial results, scattered in the literature, might hint towards the possibility that some of these gradient-type iterative algorithms may share some of the properties of Cimmino's algorithm. A precise analysis, however, has to consider also the different mathematical models used there, such as quadratic optimization over linear equations which represent the dose constraints, optimization of a penalized cost function, or other models. In this respect it is interesting to note the analysis of Barakat and Newsam (Barakat and

Newsam 1985, Section 4). Our experimental results confirm that for the clinical cases we studied, intensity patterns from the gradient method tend to be relatively smoother than those from the stochastic algorithm (e.g. simulated annealing).

IV. EXPERIMENTAL SETUP

Since most institutions where IMRT is implemented include treatment of prostate cancer as one of the disease sites, it is of general interest to compare inverse plans for this particular disease site. We selected a number of planning cases for the treatment of prostate cancer to illustrate the differences between the different mathematical planning algorithms. IMRT planning for this site has been studied extensively with a number of algorithms. In our study, we compare the results from a CORVUS IMRT system with standard MLC and Cimmino's algorithm applied to IMRT inverse planning package of the FOCUS system. The same set of contoured CT (computerized tomography) images was taken as input to both systems. We choose approximately the same geometrical point for each patient as the isocenter for all planning exercises. We specify the same dose-volume histogram constraints (DVH) for the planning target volume (PTV), bladder and rectum. The beam angles selected for the inverse planning systems are $0^o, 55^o, 90^o, 145^o, 215^o, 270^o$ and 305^o(Varian convention, Varian Medical Systems, Inc., CA), as illustrated in figure 1. A simulated annealing (COR-SA) (Webb (Webb 1989) (Webb 1993, Reprinted with corrections 2001b)(Webb 1997)(Webb 2001a)) algorithm is chosen within the CORVUS system for searching the beamlet intensity distributions. We experimented also with the other gradient algorithms within the system (Downhill, COR-DH). We found that the number of segments and monitor units required to deliver an IMRT plan are generally higher for ones obtained with the simulated annealing algorithm. The plan quality in terms of tumor dose homogeneity and critical structure sparing is somewhat better. For some of the cases of prostate cancer solvable readily with the simulated annealing algorithm, it may require more interations to obtain clinically acceptable treatment plans using the COR-DH algorithm. We include the results from these algorithms for comparison. We elected to use the built-in "sliding window" segmentation package within CORVUS for Varian MLCs for final dose analysis and comparison. For the prostate case, the optimization time required for COR-SA, COR-DH, CIM, CIM-DVH are 360 s, 300 s, 62 s and 21 s respectively on similar dual 1 Ghz processor computers.

We also chose a more complex case for experimentation and comparison, a case of oropharyngeal cancer. Structure and target definition, and dose prescription followed the guidelines set by RTOG protocol #H-0022 and is summarized in table 9. The RTOG #H-0022 protocol is aimed at testing IMRT for this disease site. The prescription is written in such a way that the total dose for each target region will be treated in the same 30 fractions. The 66 Gy region is to be treated at a dose rate of 2.2 Gy per fraction, the 60 Gy region at a rate of 2.0 Gy per fraction, and the 54 Gy region at a rate of 1.8 Gy per fraction. We used nine beam angles for all the planning: $180^o, 235^o, 270^o, 325^o, 35^o, 90^o$ and 125^o. The relative location of target volumes and some of the critical structures are shown in figure 2. For this head and neck case, the optimization time required for COR-SA, COR-DH, CIM, CIM-DVH are 420 s, 360 s, 210 s and 78 s respectively on similar dual 1 Ghz processor computers.

	Goal (Gy)	volume below(%)	volume above(%)
Gross Tumor/Lymph nodes	66	<5	–
High Risk Subclinical	60	< 5	-
Subclinical	54	< 5	-
Brainstem	<54		<5
Spinal Cord	45		0
Mandible	70		0
Unspecified Normal Tissue	72.6		0
Parotid	30		<50

(9)

Cimmino algorithm for linear inequalities(CIM) and CIM-DVH algorithm are both incorporated in an in-house system for beamlet-based inverse planning. This in-house system uses the FOCUS system for intensity segmentation and final dose calculation. This particular CIM implementation uses upper and lower dose limits for involved tumor and structures. The lower limit for the target volume is specified as the goal dose and the upper limit is 10% higher than that of the goal dose. The upper limits for the critical structures are used as the optimization upper limits. The DVH compliances are evaluated with the resulting beamlet intensities. For the implementation of CIM-DVH algorithm, the DVH constraints are input as specified in table 10. For the target volumes, upper dose volume limits are also imposed to achieve acceptable dose homogeneity. They are specified as no more than 5% of the target volumes are to receive more than 5% higher dose than the goal dose. Beam arrangements are made using the user interface of the planning system. The dose calculations are performed with the calculation engine within the system. Dose matrices to voxels due to each of the beamlets are then extracted. The resolution of the dose matrices is 3 mm. Only those voxels that intercept target volumes are included in the dose matrices extracted. The resulting intensity patterns from Cimmino's algorithm and CIM-DVH algorithm are fed back into the FOCUS system for segmentation. The "sliding window" segmentation package within FOCUS for Varian MLCs is used for this purpose for consistency with the CORVUS system. The doses from the segmented fields are calculated using the superposition-convolution algorithm and analyzed.

We compared intensity patterns (overlay with anatomy), smoothness parameters for the intensity patterns, DVHs, isodoses for selected cross-sections and the resulting number of segments and monitor units.

V. RESULTS

For the prostate case that we study we obtained plans that meet all the dose-volume constraints, as listed in the table presented in (10), from COR-SA and COR-DH of CORVUS system, and our in-house beamlet-based inverse planning system with CIM and CIM-DVH algorithms. The dose-volume histograms, in Figure 3, show that we have similar coverage of the PTV volume from the plans;

	Goal (Gy)	volume below(%)	volume above(%)
PTV	75.6	<5	–
rectum	<65	–	<20
bladder	<65	–	<20

(10)

with the plan from CORVUS covering PTV at 95% of the volume with the prescription dose and the plan from CIM and CIM-DVH algorithms covering also at 95%. The maximum doses for all these plans are around 87 Gy with about 10% of the PTV volume getting more than 85 Gy. The dose level for bladder and rectum are all acceptable with less than 20% of the organ at risk (OAR) getting more than 65 Gy. Isodose distributions for transversal, coronal and sagittal cross-sections from the plans of COR-SA, CIM algorithms are shown in Figures 4, 5, and 6, respectively (the ones from COR-DH and CIM-DVH are similar). We used addtional 3 mm margin around PTV except the posterior region where rectum is overlapping with PTV. Overall, we observe similar coverage of tumor volumes from the algorithms of the CORVUS system and the in-house system with CIM and CIM-DVH algorithms. However, for similar dose coverage from the plans, we obtained intensity patterns that are different.

Figures 7 - 10 show the intensity distributions for five level segmentations for the beam angles $0^o, 55^o, 90^o, 145^o$respectively, from COR-SA, COR-DH, in-house beamlet-based system with CIM and CIM-DVH algorithms. We observe qualitatively the differences in structure of intensity distributions from all these sources. The intensity patterns obtained with COR-DH, CIM and CIM-DVH algorithms show less irregularity than the patterns from the simulated annealing method.

To give a quantitative illustration of the smoothness comparison we analyzed beamlet intensities from all beam angles, $i = 1, 2, \ldots, m$. To do so we index the gantry angles by $g = 1, 2, \ldots, G$, and the two-dimensional beamlets location within each beam by (u, v) for $u = 1, 2, \ldots, U$, and $v = 1, 2, \ldots, V$. In this manner each beamlet index i is mapped onto the triplet (g, u, v) denoting its beam index g and the beamlet location (u, v) inside that beam. The intensity of the i-th beamlet, which was denoted by x_i in Section II, will thus be denoted by $x(g, u, v)$.

In the prostate case, shown in our example, we have seven gantry angles, i.e., $G = 7$, at angles $0^o, 55^o, 90^o, 145^o, 215^o, 270^o$ and 305^o. Within each gantry angle, we have a 2D intensity map of size 12×12, i.e., $U = V = 12$. The 2D intensity patterns $x(g, u, v)$ for $g = 1, ..., 7$ are normalized to its maximum value for that particular beam angle to take values from 0, 20, ... to 100 (the five levels). We use the smoothness indicators defined by Webb, Convery and Evans (Webb et al. 1998, p. 2787). To this end we calculate the first and second order derivatives of these normalized intensity numbers with respect to the intensity intervals for each of the beam angle, e.g.,

$$\frac{d}{dv}x(g, u, v) \text{ and } \frac{d^2}{d^2v}x(g, u, v). \tag{11}$$

Then we define the mean modulus first derivative of the beamlets as the first smoothness indicator by

$$S_1 = \frac{1}{V \times U}\sum_{v=1}^{V}\sum_{u=1}^{U} |\frac{d}{dv}x(g, u, v) \mid + \mid \frac{d}{du}x(g, u, v) \mid \tag{12}$$

and the mean modulus second derivative of the beamlets as the second smoothness indicator by

$$S_2 = \frac{1}{V \times U}\sum_{v=1}^{V}\sum_{u=1}^{U} |\frac{d^2}{d^2v}x(g, u, v)| + |\frac{d^2}{d^2u}x(g, u, v)|. \tag{13}$$

	S1				S2			
Beam Angle	COR-SA	COR-DH	CIM	CIM-DVH	COR-SA	COR-DH	CIM	CIM-DVH
0^o	18.5	12.5	10.1	9.7	16.7	12.5	8.2	8.2
55^o	14.5	8.9	10.7	9.0	13.6	7.3	9.6	7.6
90^o	14.4	10.7	10.1	8.3	12.9	10.3	9.4	7.4
145^o	15.3	14.1	13.1	8.9	14.2	13.6	11.8	7.4
215^o	16.3	14.4	11.5	8.8	14.8	13.9	9.1	6.9
270^o	14.4	12.8	9.9	8.3	13.4	12.1	9.6	7.4
305^o	12.8	7.8	10.1	8.5	11.8	7.3	8.8	7.4
Total	106	81	75	62	97	77	66	52

(14)

In table 14 we list the normalized summation of first and second derivatives of the normalized intensity numbers (11), namely, the smoothness indicators S_1 and S_2 for all the beam angles. Listed in the table are values from COR-SA, COR-CH, the ones from the in-house system with CIM and CIM-DVH algorithms. Included are values for gantry angles listed to the left of the table. There are obvious differences between the values of these smoothness indicators for the intensity patterns obtained from the CORVUS system with simulated annealing and downhill gradient and those from either the CIM or the CIM-DVH method. The smoothness values decrease with the following order: COR-SA, COR-DH, CIM and CIM-DVH, which confirms our qualitative observation from the intensity maps.

The smoothness of the intensity distribution affects the number of segments and monitor units required for delivery. While the DVHs and the isodose distributions obtained from all three methods are of similar clinical quality,table (15) shows differences in the number of segments (for each beam angle) that are required to achieve the intensity distributions shown in Figures 7 - 10. The numbers of monitor units for delivery of these segments (for each beam angle) are also listed. The monitor units are for delivery of 75.6 Gy in 42 fractions.

The delivery efficiency that can be adjusted within the CORVUS system to reduce number of segments and monitor units are not used in this case because the quality of the resulting plan in the interest of comparison. Some of the differences may lie in the different intensity segmentation software inplemented in CORVUS system and FOCUS system. However, one sees the general trend of decreased number of segments and monitor units in the same ordering: COR-SA, COR-DH and CIM/CIM-DVH.

	Segments				Monitor Units			
Beam Angle	COR-SA	COR-DH	CIM	CIM-DVH	COR-SA	COR-DH	CIM	CIM-DVH
0^o	26	14	6	7	200	264	63	83
55^o	29	13	7	5	207	169	57	66
90^o	21	18	8	6	172	136	86	80
145^o	25	17	7	5	195	55	47	44
215^o	20	25	6	5	182	97	46	42
270^o	22	25	7	5	127	98	80	78
305^o	22	11	6	7	166	174	60	65
Total	165	123	47	40	1249	992	439	458

(15)

We observe the same trend for the results of the oropharyngeal cancer. The DVH for the results from all systems are presented in two separate figures 11 and 12 in the interest of clarity. DVHs for PTV66, PTV60, PTV54, cord and parotid are presented. We observe that the target objectives of having more than 95% of the volume PTV66, PTV60, PTV54 receiving more than 66 Gy, 60 Gy and 54 Gy respectively are met by all the systems. The maximum doses for cord are all less than 45 Gy. The doses to 50% of the parotid volume are all controlled to be under 30 Gy.

The smoothness indicator S1 and S2 are also calculated for the intensity maps from all systems of all beam angles. They are listed in table 16. We observe the same trend, namely, S1 and S2 decrease in the following order: COR-SA, COR-DH, CIM and CIM-DVH.

	S1				**S2**			
Beam Angle	COR-SA	COR-DH	CIM	CIM-DVH	COR-SA	COR-DH	CIM	CIM-DVH
0^o	15.2	16.1	14.7	15.3	13.9	15.4	14.3	13.7
40^o	15.4	10.2	8.4	8.2	14.5	8.2	7.7	7.3
80^o	12.6	11.8	10.1	10.1	12.6	10.2	8.9	9.2
120^o	16.8	14.0	12.1	8.6	13.8	14.2	12.3	8.8
160^o	19.3	13.2	11.0	10.6	18.9	14.0	11.5	10.5
200^o	19.1	13.0	11.1	8.6	17.8	13.3	11.0	8.6
240^o	20.6	17.6	15.6	13.8	19.0	16.1	14.6	11.0
280^o	15.5	14.2	12.1	9.0	13.6	14.3	12.7	8.9
320^o	12.8	16.1	14.3	11.3	11.3	15.6	13.9	11.4
Total	147	126	109	95	136	121	106	89

(16)

The number of segments and monitor units required to deliver these intensity distributions are listed in table 17. Similarly, some of the difference may be explained by the different intensity segmentation software incorporated in CORVUS and FOCUS system. However, the same tendency still holds. The number of segments and monitor units decrease with the same order: COR-SA, COR-DH, CIM and CIM-DVH.

	Segments				Monitor Units			
Beam Angle	COR-SA	COR-DH	CIM	CIM-DVH	COR-SA	COR-DH	CIM	CIM-DVH
0^o	36	24	9	13	198	349	69	66
40^o	24	20	7	9	124	245	60	61
80^o	26	16	7	10	134	198	46	55
120^o	28	12	10	8	194	27	86	72
160^o	36	30	9	8	238	68	28	52
200^o	28	20	10	8	179	40	52	100
240^o	22	20	10	12	86	48	93	99
280^o	22	28	16	9	98	62	55	70
320^o	32	24	10	12	140	54	129	83
Total	256	197	88	89	1391	1091	618	658

(17)

VI. DISCUSSION

We detected this smoothness phenomenon of Cimmino's algorithm recently when working with aperture-based inverse planning (ABIP)(Xiao et al. 2003). It was discovered that Cimmino's algorithm always generated in our experimental computational work, when initialized at zero, solutions that were surprisingly good approximations of the LIF (least-square intensity feasibility) solution. This was explained and put on firm mathematical ground in the other publication(Xiao et al. 2003) . In order to achieve the least-square of the total intensity, extreme intensity values are discriminated against. The smoothness intensity patterns without large variations are thus created. In what follows we explain the *inherent smoothness property* of intensity patterns generated by Cimmino's algorithm. We consider a vector $x = (x_i)_{i=1}^m \in R^m$, translate it, in an agreed manner, into a $K \times K$ matrix (so that $m = K^2$) $X = (x_{st})_{s,t=1}^{K}$ whose elements x_{st} are obtained from the components of the vector x by $x_{st} = x_{(s-1)K+t}$, for all $s, t = 1, 2, \ldots, K$, and speak interchangeably about the vector and the associated matrix. The smoothness of the vector x (or the matrix X) is a local property that should reflect by how much does a value of one component (bixel) differ from its surrounding components' values.

A commonly used smoothness indicator $\sigma(X)$ of an image represented in a discretized form by a matrix $X = (x_{st})_{s,t=1}^{K}$ is defined by

$$\sigma(X) = (1/8) \sum_{s,t=1}^{K} \sum_{(y,z) \in N(s,t)} (x_{yz} - x_{st})^2 \tag{18}$$

where $N(s,t)$ is the set of indices of the eight surrounding elements neighborhood of the element (s,t), see, e.g., Li, Jiang and Evans (Li, Jiang and Evans 2000). Since we are interested in matrices of only nonnegative elements (intensities), this can be equivalently written as

$$\sigma(X) = (1/8) \sum_{s,t=1}^{K} \|x_{st}\mathbf{1} - \widetilde{x}\|^2 \tag{19}$$

where $\mathbf{1}$ is a nine-dimensional vector all of whose components are equal to one and $\widetilde{x}$ is a nine-dimensional vector whose components are equal to the values in the $(s,t) \cup N(s,t)$ square region. Now we show that $\sigma(X)$ is a convex function.

Proposition 2 *Given finitely many vectors x^r, for $r = 1, 2, \ldots, \rho$, we have*

$$\sigma(\sum_{r=1}^{\rho} \alpha_r x^r) \leq \sum_{r=1}^{\rho} \alpha_r \sigma(x^r), \tag{20}$$

for any set of real positive numbers α_r such that $\sum_{r=1}^{\rho} \alpha_r = 1$.

We have $\sigma(y) = (1/8) \sum_{s,t=1}^{K} \|y_{st}\mathbf{1} - \widetilde{y}\|^2$
$= (1/8) \sum_{s,t=1}^{K} \| \sum_{r=1}^{\rho} \alpha_r \left(x_{st}^r \mathbf{1} - \widetilde{x^r} \right) \|^2$
$\leq (1/8) \sum_{s,t=1}^{K} \sum_{r=1}^{\rho} \alpha_r \|x_{st}^r \mathbf{1} - \widetilde{x^r}\|^2$
$= \sum_{r=1}^{\rho} \alpha_r \sigma(x^r)$, where we have used (19) and the convexity of the function $\| \cdot \|^2$, and the proof is complete.

This shows that the smoothness indicator of any convex combination of vectors is smaller (not larger, to be precise) then the convex combination of the smoothness indicators of the individual vectors comprising the convex combination. Since Cimmino's algorithm takes convex combinations of the individual projections onto the physical dose constraints at each and every step it systematically strives to have smoother iterates.

The experiments of inverse treatment planning performed here reveal yet another important feature of the Cimmino algorithm. Namely, when comparing the intensity patterns obtained from Cimmino's algorithm with those obtained from the simulated annealing algorithm, employed by the CORVUS system, which does not have an intrinsic control over the range of intensities unless used with external filtering(Webb 1989) – the difference in smoothness of the intensity distribution is significant, as shown in Figures 7 - 10. The smoothness of the pattern is of significant clinical value because fewer segments are used for delivery and the total number of monitor units used is reduced. These effects increase the delivery efficiency and reduce the leakage radiation as compared with what would have been with a high number of monitor units. Incorporating dose-volume constraints with Cimmino's algorithm, neccessitated modifications to the modeling as well as to the iteration process which involves non-linear terms. However, we observe similar smooth patterns from the final results as compared with the CIM algorithm. The gradient algorithm is found to also share some of the smoothness features.

Besides arriving at smooth intensity distributions for beamlet-based inverse planning problems, the simultaneous property of Cimmino's algorithm makes it possible to utilize the available computing resources through parallel computing. Multithreaded implementation of the Cimmino algorithm which takes full advantage of its parallel characteristic using a double-processor computer almost halved the performance time in comparison with its sequential implementation. The simultaneous property is retained in this implementation of DVH constraints for inclusion of non-linear inequalities(Michalski et al. 2004).

VII. CONCLUSION

In implementing and experimentally analyzing Cimmino's algorithm for beamlet-based inverse planning problems, we observe an intrinsic property of the algorithm to produce smooth intensity patterns as applied to beamlet-based IMRT inverse planning which has not been observed or reported till now. The algorithm not only arrives at solutions that are close approximations of least-intensity solutions, but also generates intensity distributions that are mostly smooth. The smooth intensity pattern eases the delivery difficulty and improves delivery efficiency for both dynamic MLC and MSF–MLC delivery of the IMRT plans. Fewer segments and monitor units are required. We can reduce the optimization time many folds utilizing multiple processors due to the simultaneous nature of the algorithm. Implementation of DVH objectives in the simultaneous projection algorithm didn't seem to degrade the level of smoothness from our observation. With the debut of faster and less expensive computing hardware, real time inverse planning becomes a realty. To summarize, the combination of inequality constraints for describing the dose upper and lower limits on organs and the use of Cimmino's algorithm for the linear feasibility problem arising from the fully-discretized model of IMRT have the following favorable features and properties:

1. It uses realistic modelling, which does not require equalities to hold for the dose constraints.

2. When initialized at zero intensities it generates an approximate LIF solution (which has least intensity).

3. It converges globally to a feasible solution, if such a solution exists, or to a minimal value of the proximity function (6) in the inconsistent case.

4. It is an inherently parallel iterative algorithm, thus, implementable on parallel computing equipment regardless of problem structure.

5. It generates smoother intensity distributions.

   These properties are shared by the simultaneous projection algorithm that incorporates DVH dose objectives.

VIII. APPENDIX

The Fully Discretized Model and the Feasibility Approach

The beamlet-based inverse planning process assumes full discretization of both the patient's cross-section and the radiation intensity field surrounding the patient. Using a state-of-the-art dose calculation engine we construct a matrix of dose information in which the matrix element a_i^j is the dose to voxel j due to a unit intensity from beamlet i. We conducted our work with the inverse planning package of the commercial treatment planning system FOCUS (from Computerized Medical Systems (CMS), Inc., St. Louis, MO, USA). Having been granted access to this system's source code, we used the system as our dose calculation engine. The physician's imposed dose constraints and their respective weights of importance were also extracted from the FOCUS system. Then the Cimmino algorithm (which is not part of the FOCUS system), or the variation of the algorithm incorporating DVH dose objectives, was applied.

Next, we review how full discretization of the beamlet-based inverse problem in radiation therapy treatment planning (RTTP) leads to a linear feasibility problem and present the simultaneous Cimmino (CIM) method (Censor and Zenios 1997). Assume that the 3D volume of interest includes Q pre-identified target regions, denoted by $\{T_q \mid \text{for } q = 1, 2, \cdots, Q\}$, for radiation treatment and that the lower bounds for the required dose to be deposited in target region T_q is t_q. The volume of interest also includes S pre-identified critical organs, denoted by $\{B_s \mid \text{for } s = 1, 2, \cdots, S\}$, that should be spared by observing upper bounds of permissible dose b_s in organ B_s. The reminder of the volume constitutes the complimentary tissue, denoted by C, which is allowed to absorb not more then c dose units. This volume of interest is discretized into a Cartesian grid of n voxels which are numbered in an agreed manner by $j = 1, 2, \cdots, n$. Depending on whether a voxel is inside a target (tumor) or inside a critical organ the total dose absorbed in it must lie above or below the lower or upper prescribed dose bounds, respectively.

The RTTP problem is further discretized by assuming that the radiation, delivered from outside sources, propagates along lines and that the whole volume of interest is uniformly covered by a mesh of m lines, along which radiation travels (beamlets), densely enough to reach every voxel in the volume of interest. The beamlets are arranged in a certain geometry and indexed by $i = 1, 2, \cdots, m$. The intensities x_i of the rays are arranged in an m-dimensional vector $x = (x_i)_{i=1}^m \in R^m$, in the m-dimensional Euclidean space R^m, and they are the unknowns of the problem. These intensities are traditionally called "weights" in this field but we reserve the latter for the term "weights of importance" of the constraints. We extract the quantities a_i^j which are the dose absorbed (uniformly) in voxel j due to radiation of unit intensity along the i-th ray from the FOCUS commercial treatment planning system.

The basic *linear feasibility problem* (LFP, for short) associated with recovering the beamlet intensities vector $x = (x_i)_{i=1}^m$ is the following.

$$\sum_{i=1}^{m} a_i^j x_i \leq b_s, \quad \text{for all} \quad j \in B_s, \quad s = 1, 2, \cdots, S, \tag{21}$$

$$t_q \leq \sum_{i=1}^{m} a_i^j x_i, \quad \text{for all} \quad j \in T_q, \ q = 1, 2, \cdots, Q, \tag{22}$$

$$\sum_{i=1}^{m} a_i^j x_i \leq c, \quad \text{for all} \quad j \in C, \tag{23}$$

$$x_i \geq 0, \quad \text{for all} \quad i = 1, 2, \cdots, m. \tag{24}$$

The LFP can easily be rearranged into the general form

$$\sum_{i=1}^{m} a_i^j x_i \leq d_j, \quad \text{for all} \quad j = 1, 2, \cdots, n, \tag{25}$$

which can also be rewritten as

$$\langle a^j, x \rangle \leq d_j, \quad \text{for all} \quad j = 1, 2, \cdots, n, \tag{26}$$

where $a^j = (a_i^j)_{i=1}^m$ is an m-dimensional vector and $\langle a^j, x \rangle = \sum_{i=1}^m a_i^j x_i$ is the inner product in R^m. The nonnegativity constraints (24) can be either subsumed in the system (26) or kept separately and handled separately by any iterative algorithm applied to the LFP.

In order to incorporate the dose-volume histogram constraints, we use an additional set of inequalities, the detail of which is described in a recent publication (Michalski et al. 2004). A brief summary of the modeling is included. For each structure s containing N_s voxels we have a set of constraints T^s. For $t \in T^s$, we are allowing α_t percent volume getting an over dose of β_t percent of the upper limit b_t (similar set of inequalities can be constructed for lower limits):

$$\langle a^j, x\rangle \leq (1+\beta_t)b_t, \quad \text{for all} \quad j = 1, 2, \cdots, N_s, \tag{27}$$

$$g_t(x) = \sum_{j \in s} h_j(x) - \alpha_t N_s b_t \beta_t \leq 0 \tag{28}$$

$$h_j(x) = \begin{cases} 0 \text{ if } \langle a^j, x\rangle \leq b_t \\ \langle a^j, x\rangle - b_t\beta_t + b_t \text{ if } b_t \leq \langle a^j, x\rangle \leq (1+\beta_t)b_t \\ \langle a^j, x\rangle - b_t \text{ if } \langle a^j, x\rangle > (1+\beta_t)b_t \end{cases} \tag{29}$$

Non-linear terms are introduced in the inequalities to accommodate the dose-volume constraints.

Acknowledgments. *This work was supported in part by* Elekta Oncology Systems Inc., Norcross, GA, USA. *The work of Y. Censor was supported by research grant 592/00 from the Israel Science Foundation founded by the Israel Academy of Sciences and Humanities. We gratefully acknowledge the help rendered to this research by Computerized Medical Systems (CMS), St. Louis, MO, USA, by giving us access to some source code of FOCUS treatment system software.*

REFERENCES

Aharoni, R. and Censor, Y.: 1989, Block-iterative projection methods for parallel computation of solutions to convex feasibility problems, *Linear Algebra and Its Applications* **120**, 165–175.

Alber, M. and Nusslin, F.: 2000, Intensity modulated photon beams subject to a minimal surface smoothing constraint, *Physics in Medicine and Biology* **45**, N49–N52.

Altschuler, M. D. and Censor, Y.: 1984, Feasibility solutions in radiation therapy treatment planning, *Proceedings of the Eighth International Conference on the Use of Computers in Radiation Therapy*, IEEE Computer Society Press, Silver Spring, Maryland, USA, pp. 220–224.

Auslender, A.: 1976, *Optimization: Méthodes Numériques*, Masson, Paris, France.

Barakat, R. and Newsam, G.: 1985, Algorithms for reconstruction of partially known, bandlimited Fourier tarnsform pairs from noisy data. II. The nonlinear problem of phase retrival, *Journal of Integral Equations* **9 (Suppl.)**, 77–125.

Bauschke, H. and Borwein, J.: 1996, On projection algorithms for solving convex feasibility problems, *SIAM Review* **38**, 367–426.

Bednarz, G., Michalski, D., Houser, C., Huq, M. S., Xiao, Y., Anne, P. R. and Galvin, J. M.: 2002, The use of mixed-integer programming for inverse treatment planning with pre-defined field segments, *Phys. Med. Biol.* **47**, 2235–2245.

Bortfeld, T., Bürkelbach, J., Boesecke, R. and Schlegel, W.: 1990, Methods of image reconstruction from projections applied to conformation radiotherapy, *Physics in Medicine and Biology* **35**, 1423–1434.

Butnariu, D., Censor, Y. and Reich, S. (eds): 2001, *Inherently Parallel Algorithms in Feasibility and Optimization and Their Applications*, Vol. 8 of *Studies in Computational Mathematics*, Elsevier Science B.V., Amsterdam, The Netherlands.

Byrne, C. and Censor, Y.: 2001, Proximity function minimization using multiple Bregman projections, with applications to split feasibility and Kullback-Leibler distance minimization, *Annals of Operations Research* **105**, 77–98.

Censor, Y., Altschuler, M. D. and Powlis, W. D.: 1988a, A computational solution of the inverse problem in radiation therapy treatment planning, *Applied Mathematics and Computation* **25**, 57–87.

Censor, Y., Altschuler, M. D. and Powlis, W. D.: 1988b, On the use of Cimmino's simultaneous projections method for computing a solution of the inverse problem in radiation therapy treatment planning, *Inverse Problems* **4**, 607–623.

Censor, Y. and Zenios, S.: 1997, *Parallel Optimization: Theory, Algorithms, and Applications*, Oxford University Press, New York, NY, USA.

Cho, P., Lee, S., Marks, R., Oh, S., Sutlief, S. and Phillips, M.: 1998, Optimization of intensity modulated beams with volume constraints using two methods: Cost function minimization and projection onto convex sets, *Medical Physics* **25**, 435–443.

Cho, P., Lee, S., Marks, R., Redstone, J. and Oh, S.: 1997, Comparison of algorithms for intensity modulated beam optimization: Projection onto convex sets and simulated annealing, *in* D. Leavitt and G. Starkschall (eds), *Proceedings of the XII International Conference On the Use of Computers in Radiation Therapy*, Medical Physics Publishing, Madison, WI, USA, pp. 310–312.

Cho, P. and Marks, R. I.: 2000, Hardware-sensitive optimization for intensity modulated radiotherapy, *Physics in Medicine and Biology* **45**, 429–440.

Cimmino, G.: 1938, Calcolo approssimato per le soluzioni dei sistemi di equazioni lineari, *La Ricerca Scientifica XVI, Series II, Anno IX,* **1**, 326–333.

Haas, O.: 1999, *Radiotherapy Treatment Planning: New System Approaches*, Springer-Verlag, London.

Hiriart-Urruty, J.-B. and Lemarechal, C.: 2001, *Fundamentals of Convex Analysis*, Springer-Verlag, Berlin, Heidelberg, Germany.

Höffner, J., Decker, P., Schmidt, E., Herbig, W., Ritter, J. and Wiss, P.: 1996, Development of a fast optimization preview in radiation treatment planning, *Strahlentherapie und Onkologie* **172**, 384–394.

Kolmonen, P., Trevo, J. and Lahtinen, T.: 1998, Use of Cimmino algorithm and continuous approximation for the dose deposition kernel in the inverse problem of radiation treatment planning, *Physics in Medicine and Biology* **43**, 2539–2554.

Lee, S., Cho, P., II, R. M. and Oh, S.: 1997, Conformal radiotherapy computation by the method of alternating projections onto convex sets, *Physics in Medicine and Biology* **42**, 1065–1086.

Li, X., Jiang, T. and Evans, D. J.: 2000, Medical image reconstruction using a multi-objective genetic local search algorithm, *International Journal of Computer Mathematics* **74**, 301–314.

Michalski, D., Xiao, Y., Censor, Y. and Galvin, J. M.: 2004, The dose-volume constraint satisfaction problem for inverse treatment planning with field segments, *Physics in Medicine and Biology* **49**, 601–616.

Powlis, W., Altschuler, M., Censor, Y. and Buhle, E.: 1989, Semi-automated radiotherapy treatment planning with a mathematical model to satisfy treatment goals, *International Journal Radiation Oncology Biology Physics* **16**, 271–276.

Spirou, S. and Chui, C.-S.: 1998, A gradient inverse planning algorithm with dose-volume constraints, *Medical Physics* **25**, 321–333.

Spirou, S., Fournier-Bidoz, N., Yang, J., Chui, C.-S. and Ling, C.: 2001, Smoothing intensity-modulated beam profiles to improve the efficiency of delivery, *Medical Physics* **28**, 2105–2112.

Stark, H. and Yang, Y.: 1998, *Vector Space Projections: A Numerical Approach to Signal and Image Processing, Neural Nets, and Optics*, John Wiley, New York, NY, USA.

Starkschall, G.: 1984, A constrained least-squares optimization method for external beam radiation therapy treatment planning, *Medical Physics* **11**, 659–665.

Webb, S.: 1989, Optimisation of conformal radiotherapy dose distributions by simulated annealing, *Physics in Medicine and Biology* **34**, 1349–1369.

Webb, S.: 1993, Reprinted with corrections 2001b, *The Physics of Three-Dimensional Radiation Therapy*, Institute of Physics Publishing (IOP), Bristol, UK.

Webb, S.: 1997, *The Physics of Conformal Radiotherapy*, Institute of Physics Publishing (IOP), Bristol, UK.

Webb, S.: 2001a, *Intensity-Modulated Radiation Therapy*, Institute of Physics Publishing (IOP), Bristol, UK.

Webb, S., Convery, D. J. and Evans, P. M.: 1998, Inverse planning with constraints to generate smoothed intensity-modulated beams, *Physics in Medicine and Biology* **43**, 2785–2794.

Wu, C., Jeraj, R., Lu, W. and Mackie, T. R.: 2004, Fast treatment plan modification with an over-relaxed cimmino algorithm, *Med. Phys.* **31**(2), 191–200.

Xia, P. and Verhey, L.: 1998, Multileaf collimator leaf-sequencing algorithm for intensity modulated beams with multiple static segments, *Medical Physics* **25**, 1424–1434.

Xiao, Y., Censor, Y., Michalski, D. and Galvin, J. M.: 2003, The least-intensity feasible solution for aperture-based inverse planning in radiation therapy, *Annals of Operations Research* **119**, 183–203.

Xiao, Y., Galvin, J. M., Hossain, M. and Valicenti, R.: 2000, An optimized forward-planning technique for intensity modulated radiation therapy, *Medical Physics* **9**, 2093–2099.

Xing, L. and Chen, T.: 1996, Iterative methods for inverse treatment planning, *Physics in Medicine and Biology* **41**, 2107–2123.

Xing, L., Hamilton, R., Spelbring, D., Pelizzari, C., Chen, G. and Boyer, A.: 1998, Fast iterative algorithms for three-dimensional inverse treatment planning, *Medical Physics* **25**, 1845–1849.

FIGURES

FIG. 1. The seven beam angles used in the IMRT inverse planning are: 0, 55, 90, 145, 215, 270, 305 degrees (Varian convention).

FIG. 2. The relative locations of the target volumes PTV66, PTV60, PTV54 and critical structures: cord and parotid.

FIG. 3. DVH comparison between beamlet-based IMRT plans: COR-SA,COR-DH, algorithms CIM and CIM-DVH.

FIG. 4. Isodose distribution comparison between CORVUS system (upper), in-house algorithms CIM (lower) for transversal cross-section. The two isodose displays are for 75.6 Gy and 65 Gy respectively.

FIG. 5. Isodose distribution comparison between CORVUS system (upper), in-house algorithms CIM (lower) coronal cross-section. The two isodose displays are for 75.6 Gy and 65 Gy respectively.

FIG. 6. Isodose distribution comparison between CORVUS system (upper), in-house algorithms CIM (lower) for sagital plane. The two isodose displays are for 75.6 Gy and 65 Gy respectively.

FIG. 7. Intensities from left to right for: COR-SA, COR-DH, algorithms CIM and CIM-DVH shown with outline of PTV for gantry angle 0 degree.

FIG. 8. Intensities from left to right for: COR-SA, COR-DH, algorithms CIM and CIM-DVH shown with outline of PTV for gantry angle 55 degree.

FIG. 9. Intensities from left to right for: COR-SA, COR-DH, algorithms CIM and CIM-DVH shown with outline of PTV for gantry angle 90 degree.

FIG. 10. Intensities from left to right for: COR-SA, COR-DH, algorithms CIM and CIM-DVH shown with outline of PTV for gantry angle 145 degree.

FIG. 11. DVH results for the oropharygeal case from COR-SA and CIM for PTV66, PTV60, PTV54, cord and parotid.

FIG. 12. DVH results for the oropharygeal case from COR-DH and CIM-DVH for PTV66, PTV60, PTV54, cord and parotid.

Figures for the Manuscript:

Inherent Smoothness of Intensity Patterns for Intensity Modulated Radiation Therapy Generated by a Simultaneous Projection Algorithm

Y. Xiao[1], D. Michalski[1], Y. Censor[2] and J. M. Galvin[1]
[1]Medical Physics Division,
Radiation Oncology Department,
Thomas Jefferson University Hospital,
10th and Locust Streets, Philadelphia,
PA. 19107, USA.
({ying.xiao, darek.michalski, james.galvin}@mail.tju.edu).
[2]Department of Mathematics,
University of Haifa, Mt. Carmel,
Haifa 31905, Israel.
(yair@math.haifa.ac.il).

May, 2004

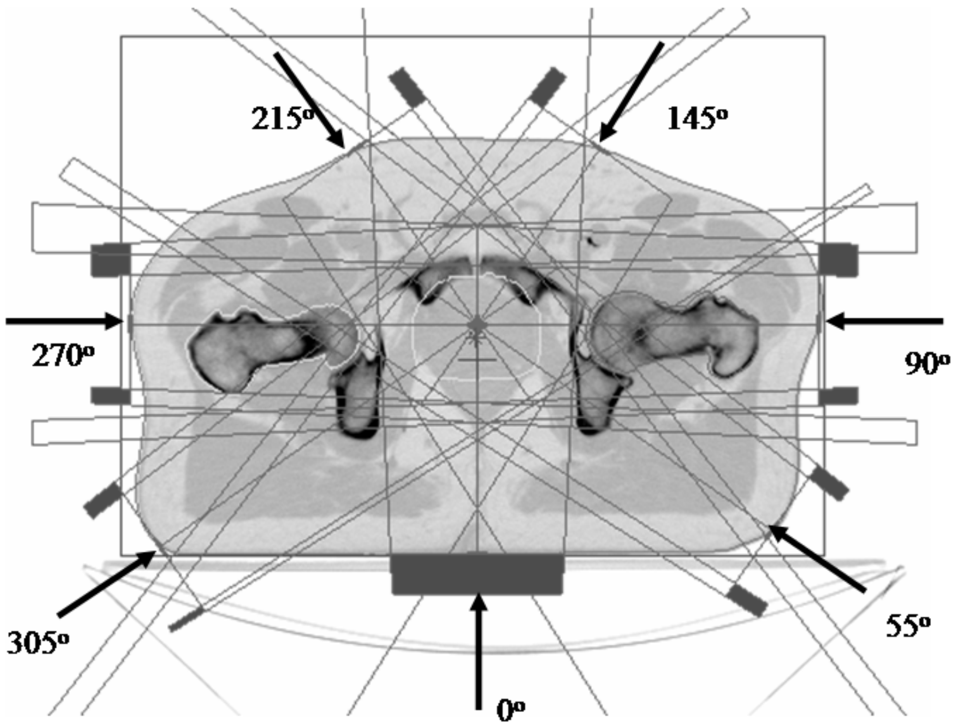

Figure 1: The seven beam angles used in the IMRT inverse planning are: 0, 55, 90, 145, 215, 270, 305 degrees (Varian convention).

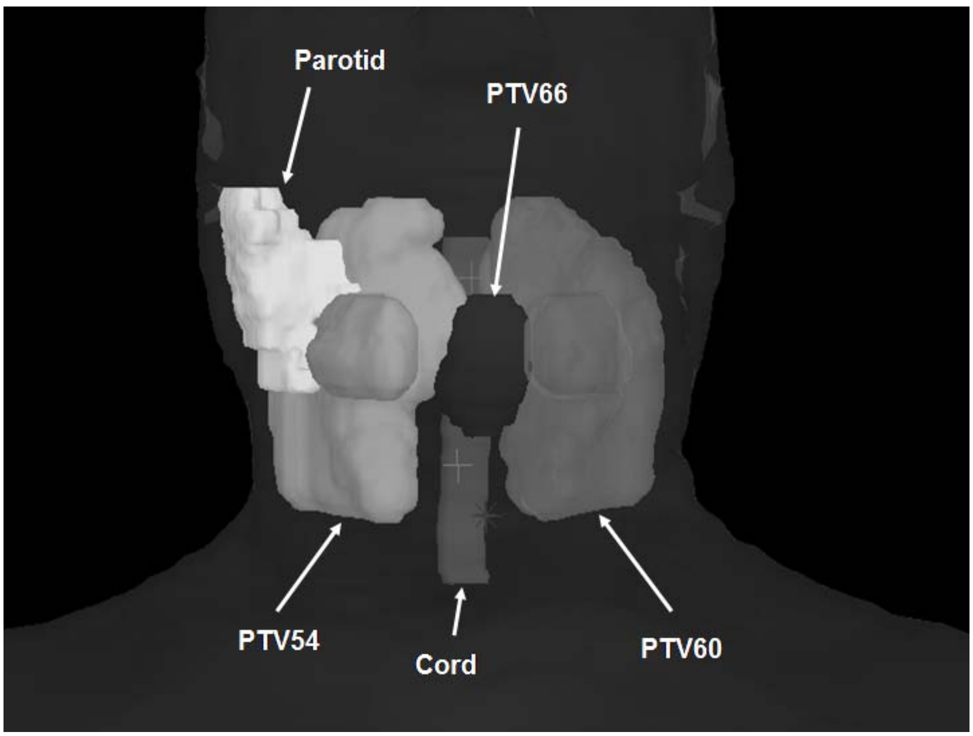

Figure 2: The relative locations of the target volumes PTV66, PTV60, PTV54 and critical structures: cord and parotid.

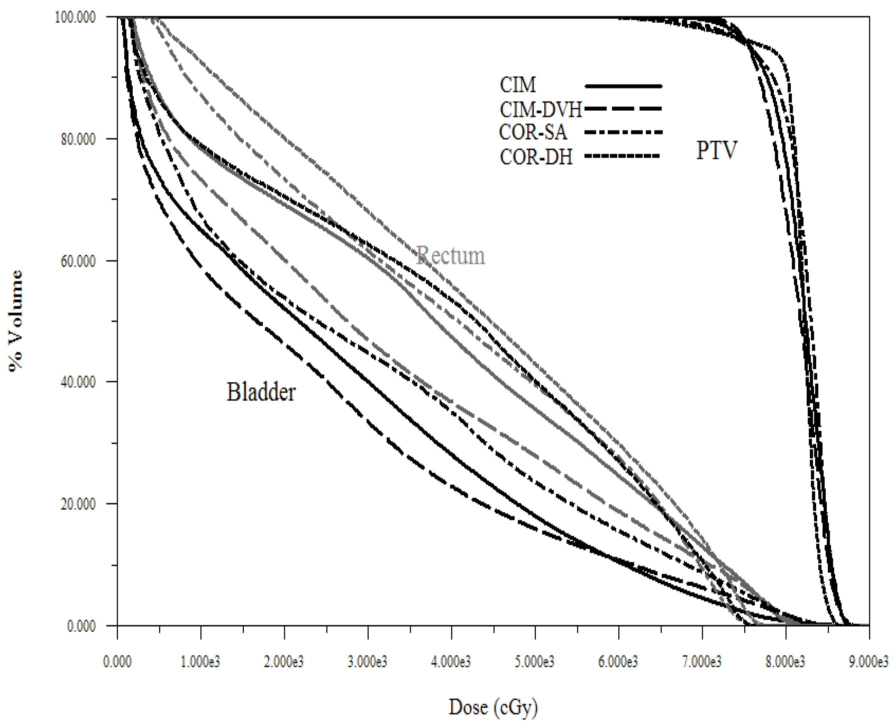

Figure 3: DVH comparison between beamlet-based IMRT plans: COR-SA,COR-DH, algorithms CIM and CIM-DVH.

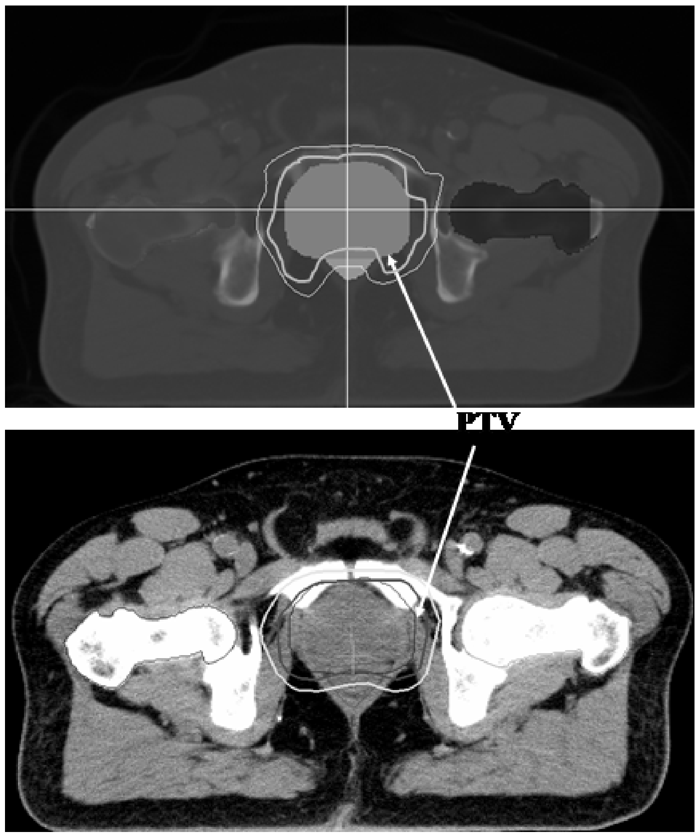

Figure 4: Isodose distribution comparison between CORVUS system (upper), in-house algorithms CIM (lower) for transversal cross-section. The two isodose displays are for 75.6 Gy and 65 Gy respectively.

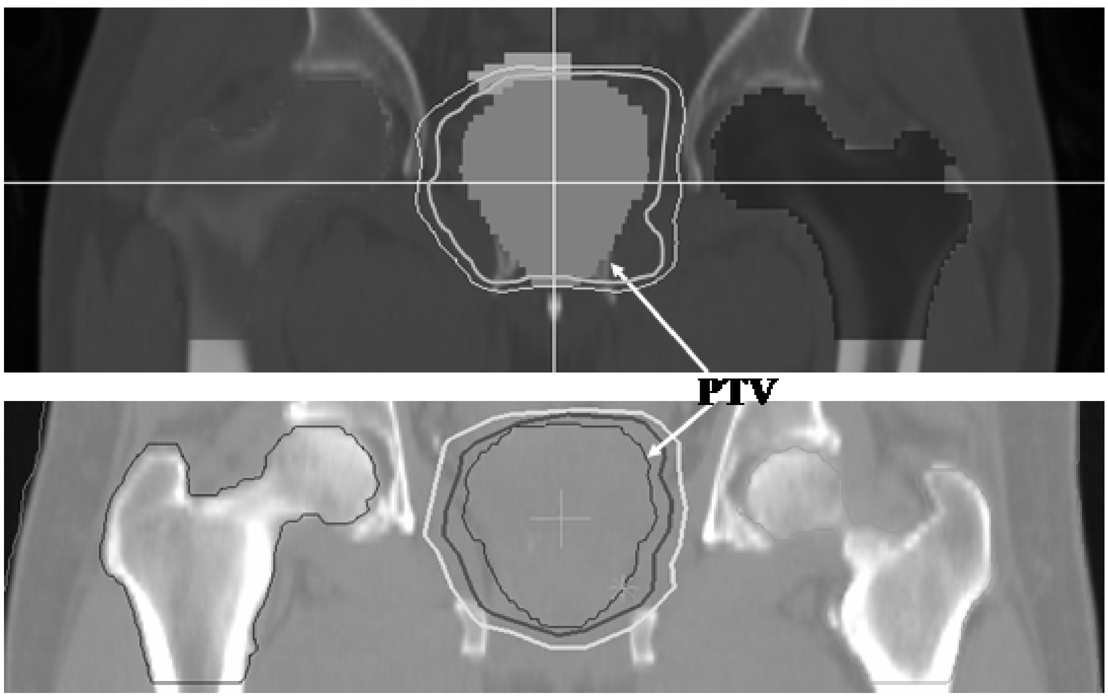

Figure 5: Isodose distribution comparison between CORVUS system (upper), in-house algorithms CIM (lower) coronal cross-section. The two isodose displays are for 75.6 Gy and 65 Gy respectively.

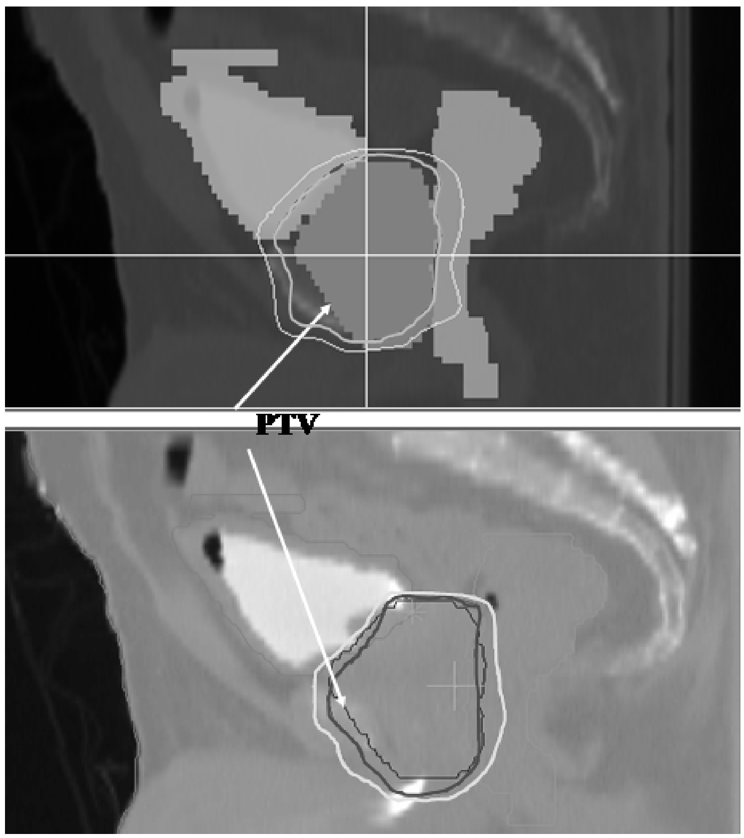

Figure 6: Isodose distribution comparison between CORVUS system (upper), in-house algorithms CIM (lower) for sagital plane. The two isodose displays are for 75.6 Gy and 65 Gy respectively.

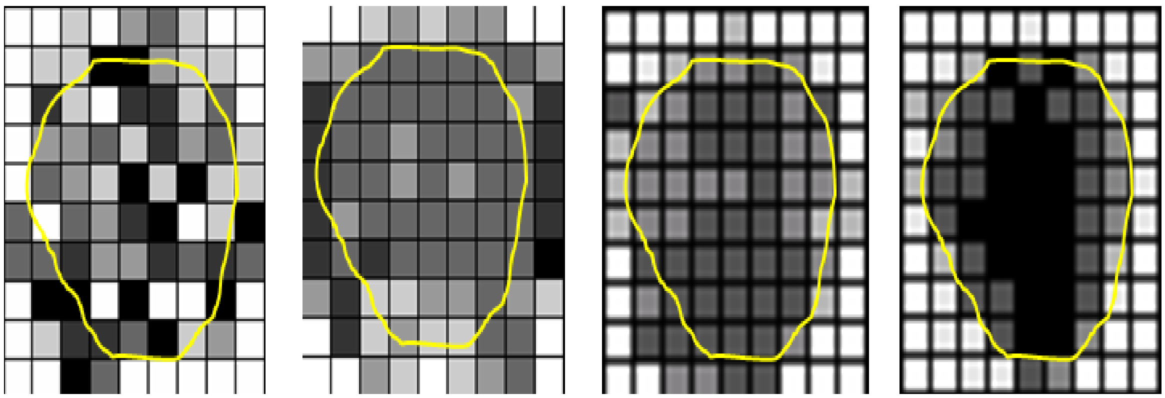

Figure 7: Intensities from left to right for: COR-SA, COR-DH, algorithms CIM and CIM-DVH shown with outline of PTV for gantry angle 0 degree.

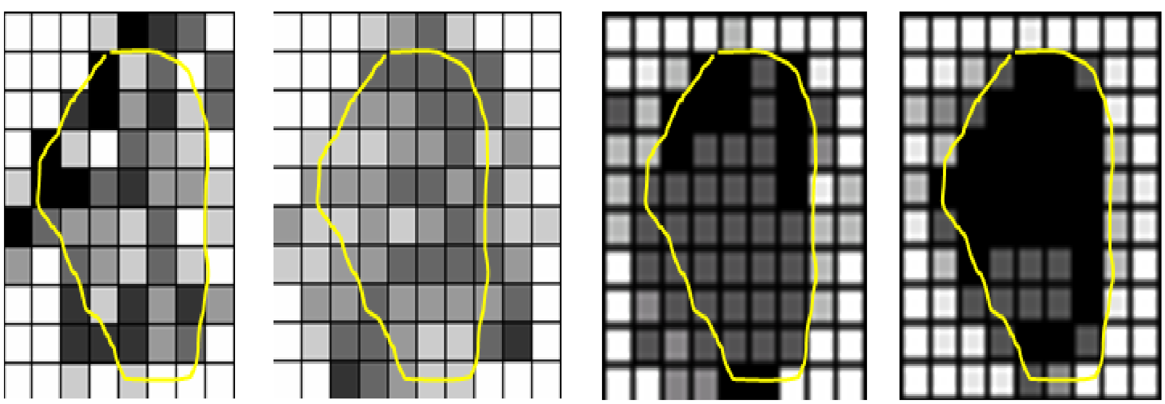

Figure 8: Intensities from left to right for: COR-SA, COR-DH, algorithms CIM and CIM-DVH shown with outline of PTV for gantry angle 55 degree.

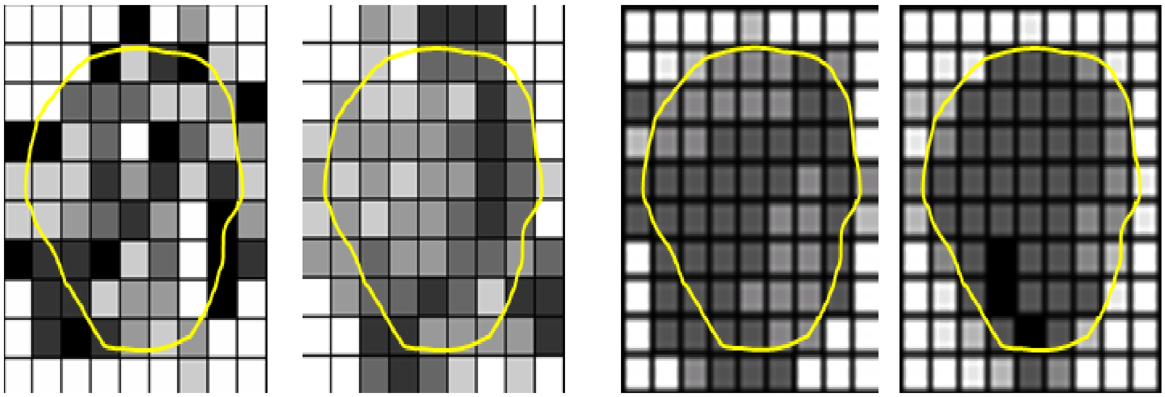

Figure 9: Intensities from left to right for: COR-SA, COR-DH, algorithms CIM and CIM-DVH shown with outline of PTV for gantry angle 90 degree.

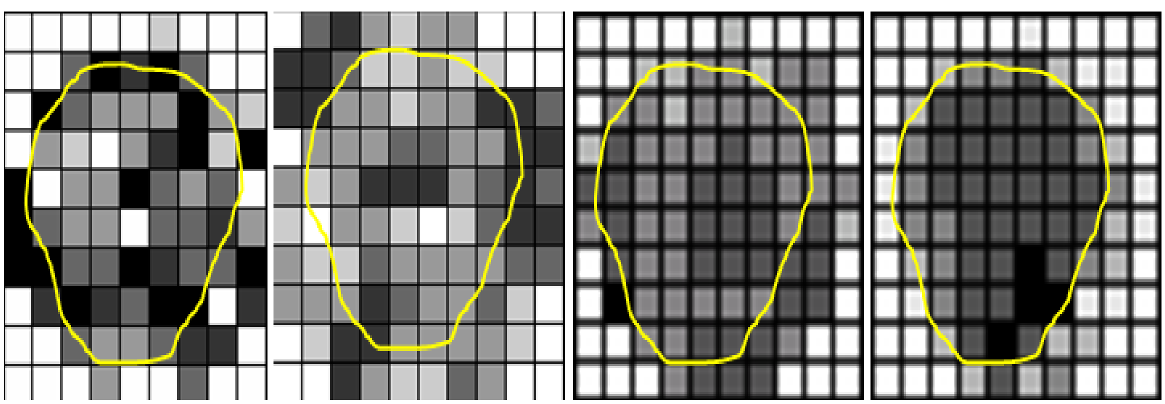

Figure 10: Intensities from left to right for: COR-SA, COR-DH, algorithms CIM and CIM-DVH shown with outline of PTV for gantry angle 145 degree.

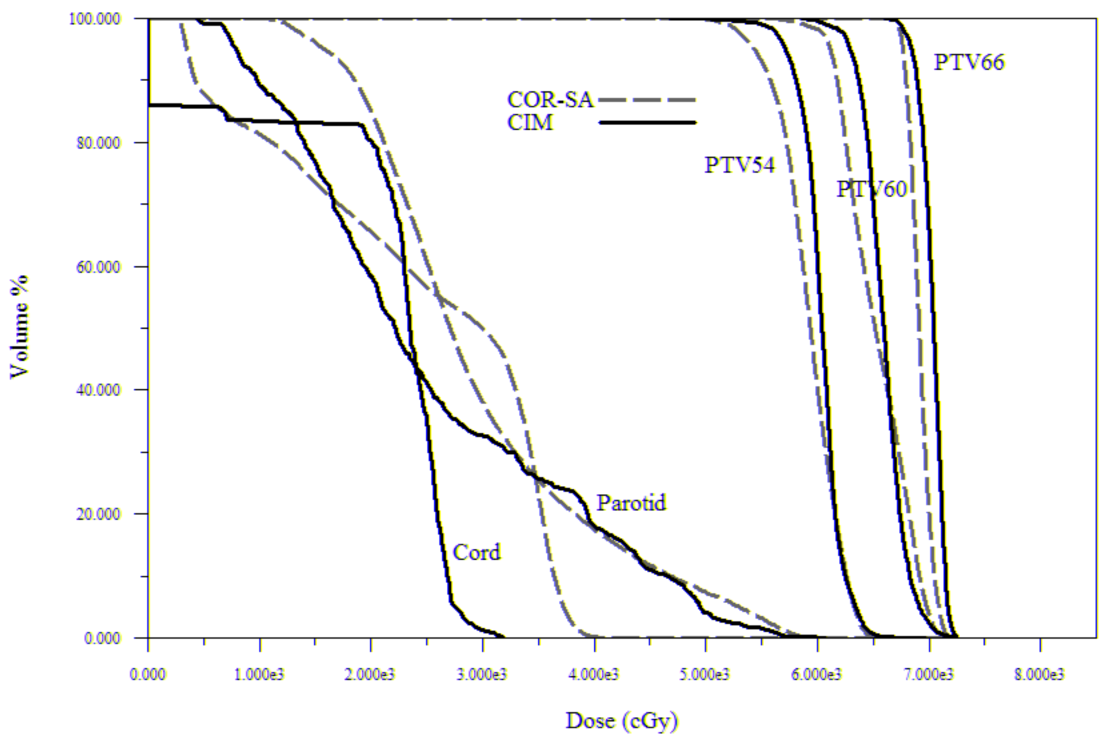

Figure 11: DVH results for the oropharygeal case from COR-SA and CIM for PTV66, PTV60, PTV54, cord and parotid.

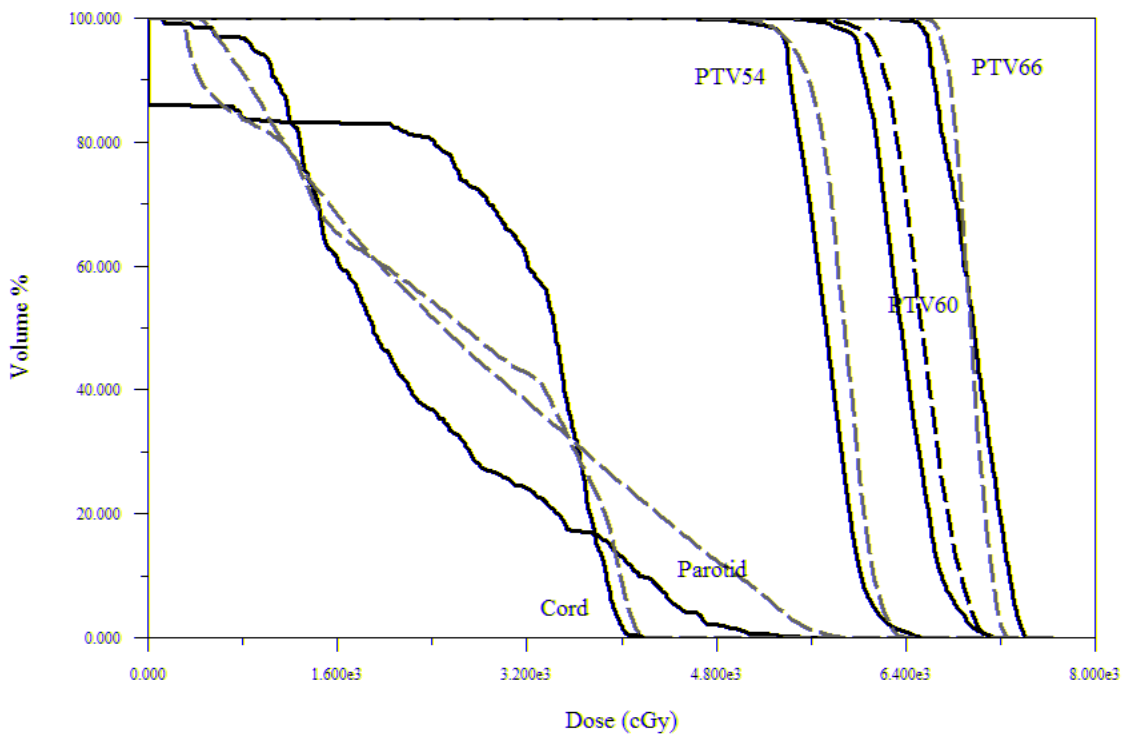

Figure 12: DVH results for the oropharygeal case from COR-DH and CIM-DVH for PTV66, PTV60, PTV54, cord and parotid.